Catheterization alters bladder ecology to potentiate *Staphylococcus aureus* infection of the urinary tract

Jennifer N. Walker[a,b], Ana L. Flores-Mireles[a,b], Chloe L. Pinkner[a,b], Henry L. Schreiber IV[a,b], Matthew S. Joens[c], Alyssa M. Park[d,1], Aaron M. Potretzke[d,2], Tyler M. Bauman[d], Jerome S. Pinkner[a,b], James A. J. Fitzpatrick[c], Alana Desai[d], Michael G. Caparon[a,b,3], and Scott J. Hultgren[a,b,3]

[a]Department of Molecular Microbiology, Washington University School of Medicine, St. Louis, MO 63110; [b]Center for Women's Infectious Disease Research, Washington University School of Medicine, St. Louis, MO 63110; [c]Center for Cellular Imaging, Washington University School of Medicine, St. Louis, MO 63110; and [d]Division of Urologic Surgery, Washington University School of Medicine, St. Louis, MO 63110

Contributed by Scott J. Hultgren, August 15, 2017 (sent for review May 8, 2017; reviewed by Michael S. Gilmore and Neal D. Hammer)

Methicillin-resistant *Staphylococcus aureus* (MRSA) is an emerging cause of catheter-associated urinary tract infection (CAUTI), which frequently progresses to more serious invasive infections. We adapted a mouse model of CAUTI to investigate how catheterization increases an individual's susceptibility to MRSA UTI. This analysis revealed that catheterization was required for MRSA to achieve high-level, persistent infection in the bladder. As shown previously, catheter placement induced an inflammatory response resulting in the release of the host protein fibrinogen (Fg), which coated the bladder and implant. Following infection, we showed that MRSA attached to the urothelium and implant in patterns that colocalized with deposited Fg. Furthermore, MRSA exacerbated the host inflammatory response to stimulate the additional release and accumulation of Fg in the urinary tract, which facilitated MRSA colonization. Consistent with this model, analysis of catheters from patients with *S. aureus*-positive cultures revealed colocalization of Fg, which was deposited on the catheter, with *S. aureus*. Clumping Factors A and B (ClfA and ClfB) have been shown to contribute to MRSA–Fg interactions in other models of disease. We found that mutants in *clfA* had significantly greater Fg-binding defects than mutants in *clfB* in several in vitro assays. Paradoxically, only the ClfB$^-$ strain was significantly attenuated in the CAUTI model. Together, these data suggest that catheterization alters the urinary tract environment to promote MRSA CAUTI pathogenesis by inducing the release of Fg, which the pathogen enhances to persist in the urinary tract despite the host's robust immune response.

host–pathogen interactions | MRSA CAUTI | ClfB–fibrinogen interactions

As *Staphylococcus aureus* only accounts for between 0.5 and 2% of all urine positive cultures, the gram-positive pathogen is not typically considered a major cause of urinary tract infection (UTI) (1–3). However, recent epidemiologic studies indicate that *S. aureus* is an emerging cause of UTI in special patient populations, such as pregnant women and those with complicated UTI (4–10). Complicated *S. aureus* UTIs are predominately associated with the presence of foreign bodies (i.e., urinary catheters or kidney stones) (4, 9, 11, 12), recent hospital exposure (8), residence in a long-term care facility (6, 13), and other comorbidities such as prostatic abscesses following prostatitis, diabetes, and cancer (14, 15). Of particular concern, complicated *S. aureus* UTIs are frequently associated with the development of severe sequelae, leading to increased rates of morbidity and mortality (4, 6, 8, 12, 13, 16–18). Additionally, treatment of these infections has become increasingly difficult, as most *S. aureus* isolates causing complicated UTI are methicillin-resistant *S. aureus* (MRSA) and are refractory to treatment by antibiotics that typically have efficacy in the urinary tract (4, 8, 12, 19, 20). This highlights the need for developing a greater understanding of the pathogenesis of complicated UTI for the development of new antibiotic-sparing therapies.

The most significant risk factor for developing complicated MRSA UTI is urinary catheterization (4, 8, 9, 12, 21). Recent studies have highlighted that in contrast to catheter-associated UTI (CAUTI) caused by other bacteria, MRSA dissemination to bacteremia following bacteriuria occurs more frequently (5 vs. 20%, respectively) and manifests rapidly, typically within 2 d of a urine positive culture (4, 12, 22). Overall, CAUTI is the leading cause of secondary hospital-associated bloodstream infections (BSIs) (23), and MRSA BSIs are associated with high rates of morbidity and mortality, frequently resulting in metastatic infections of other organs and tissues, endocarditis, and septic shock (4, 8, 12, 18, 24, 25). While MRSA invasive diseases are under intense study, the mechanisms MRSA employs to cause CAUTI remain uncharacterized. Elucidating these mechanisms will provide important insights that may be used to identify patient factors for developing invasive disease, determine effective treatment options, and understand the factors that contribute to poor patient outcomes.

Previous studies have shown that the placement of a catheter into the bladder leads to a specific and localized inflammatory response resulting in the release of the host protein fibrinogen (Fg), which accumulates in the bladder and on the catheter (26). Further, urinary catheters removed from humans have been shown to be coated with Fg (27). It has long been recognized that

Significance

***Staphylococcus aureus* is a cause of catheter-associated urinary tract infections (CAUTIs). *S. aureus* CAUTIs are problematic because they are usually caused by antibiotic-resistant strains, and patients who develop these infections have a high risk of developing serious complications. Catheterization in humans and mice causes damage in the bladder that results in the release of host protein fibrinogen (Fg). This study suggests that *S. aureus* exploits the presence of Fg via interactions mediated by the Fg-binding protein ClfB to facilitate colonization of the bladder and the catheter to cause a persistent infection in both mice and humans. Insights into *S. aureus* CAUTI pathogenesis is facilitating the development of more-targeted therapies to better treat these infections.**

Author contributions: J.N.W., A.L.F.-M., A. M. Park, A. M. Potretzke, T.M.B., J.S.P., J.A.J.F., A.D., M.G.C., and S.J.H. designed research; J.N.W., A.L.F.-M., C.L.P., and M.S.J. performed research; J.N.W. and M.S.J. contributed new reagents/analytic tools; J.N.W., A.L.F.-M., and H.L.S. analyzed data; and J.N.W., M.S.J., J.A.J.F., M.G.C., and S.J.H. wrote the paper.

Reviewers: M.S.G., Harvard Medical School; and N.D.H., Michigan State University.

The authors declare no conflict of interest.

Freely available online through the PNAS open access option.

[1]Present address: Department of Urology, Geisinger Medical Center, Danville, PA 17822.

[2]Present address: Department of Urology, Mayo Clinic, Rochester, MN 55905.

[3]To whom correspondence may be addressed. Email: caparon@wustl.edu or hultgren@wustl.edu.

This article contains supporting information online at www.pnas.org/lookup/suppl/doi:10.1073/pnas.1707572114/-/DCSupplemental.

Downloaded at Palestinian Territory, occupied on December 15, 2021

www.manaraa.com

MRSA interactions with Fg are critical in pathogenesis (28–33). For example, MRSA–Fg interactions, which result in bacterial agglutination, have been shown to contribute to pathogenesis by providing a microenvironment permissive for activation of the *agr*-quorum sensing system (34). This results in the up-regulation of virulence factors essential for survival and dissemination (34, 35). The findings that urinary catheterization alters the UT environment by triggering the release of Fg (26) and that MRSA UTI is predominately associated with urinary catheterization (26, 36–38) suggest that MRSA may exploit the presence of this host protein to cause disease. Additionally, this process is known to be true for *Enterococcus faecalis*, which expresses an endocarditis- and biofilm-associated (Ebp) pilus that is tipped with the Fg-binding protein EbpA. EbpA binding to Fg facilitates *E. faecalis* biofilm formation on the catheter, which initiates the CAUTI pathogenic cascade. While MRSA does not encode pili, the pathogen uses a large family of structurally homologous, cell wall-linked adhesin proteins, termed "microbial surface components recognizing adhesive matrix molecules" (MSCRAMMs), to interact with Fg and other host proteins to promote pathogenesis (32, 39–41).

In this study, we developed a mouse model of MRSA CAUTI to determine whether the presence of Fg during urinary catheterization creates a suitable environment for MRSA colonization and persistence. We found that (*i*) the presence of a catheter is required for persistent MRSA UTI; (*ii*) MRSA binds to regions of the catheter that are coated with Fg in both mice and humans; (*iii*) MRSA actively promotes catheter-induced inflammation to stimulate the accumulation of Fg; and (*iv*) MRSA can persist during long-term catheterization despite the presence of a robust inflammatory response. Finally, analysis of the two best-characterized Fg-binding MSCRAMMs, Clumping Factor A (ClfA) and Clumping Factor B (ClfB) (32, 39–41), revealed ClfB was important for CAUTI, supporting a mechanism whereby MRSA exploits the presence of Fg to cause persistent CAUTI.

Results

MRSA Survives and Grows in Human Urine. MRSA UTI is rare in otherwise healthy individuals, with the majority associated with catheterization (1–4, 8, 9, 12, 21). Therefore, we tested whether the low incidence of MRSA UTI was due to an inability of MRSA to grow in urine (Fig. S1). A panel of MRSA strains from diverse isolation sites (Table S1) was cultured in either rich media or pooled human urine ranging from pH 5.0 to 7.0 and growth was assessed by measuring the OD_{600} over time and determining the CFUs after 24 h. Strains JE2-MRSA, SSTI-MRSA, Co-MRSA, MRSA 1369, PUTS-1, and TOP6-555 all displayed similar growth curves in rich media, with maximal growth reaching an OD_{600} of >1.0 (Fig. S1 *A–F*) and ~10^{10} CFUs per mL after 24 h (Fig. S1*G*). All six strains also displayed similar growth curves to each other when grown in urine of any pH; however, maximal growth only reached an OD_{600} of ~0.5 (Fig. S1 *A–F*), with 1 to 5 × 10^8 CFUs per mL (Fig. S1*G*), about 1.5 logs lower than rich media. These data show that despite having reduced available nutrients, MRSA readily grows in human urine.

MRSA Requires a Catheter for Urinary Tract Colonization. Next, we investigated whether MRSA pathogenesis in the UT is potentiated by the presence of a catheter by adapting a CAUTI mouse model. A small piece of silicone tubing (implant) was transurethrally placed in the bladder before transurethral inoculation with 10^7 CFUs of MRSA 1369, PUTS-1, or TOP6-555. Control mice did not receive the implant. In the absence of an implant, 1 d post infection (dpi), mice infected with MRSA 1369, PUTS-1, or TOP6-555 all displayed a relatively low bacterial burden, albeit variable, with a mean average of approximately 10^3 CFUs (Fig. 1). In contrast, mice that received implants had bladder burdens that were 3 logs higher than nonimplanted mice (Fig. 1). MRSA 1369 was selected for further characterization in this model as it is a methicillin-resistant urine isolate and is representative of what is seen causing CAUTI in the clinic. MRSA 1369 was assessed for UT colonization and dissemination over the course of a 2-wk experiment (Fig. 2). Implanted bladders all sustained high levels of MRSA 1369 colonization with mean values greater than 10^5 CFUs (Fig. 2*A*). Retrieved implants all had high levels of colonization with mean values higher than 10^5 CFUs (Fig. 2*B*) and were associated with high bladder burdens. However, due to the nature of this model, mice occasionally lose their implant during micturition. Mice that lost the implant had significantly lower bladder bacterial burdens over 2 wk compared with mice that maintained the implant (Fig. 2*A*). Additionally, the loss of an implant early was associated with a significant decrease in bacterial burden, an effect that became less pronounced when the implant was lost later in time (Fig. 2*A*). Kidneys of mice with implants also displayed higher burdens compared with those that lost the implant by 14 dpi (Fig. 2*C*). MRSA disseminated to the blood (Fig. 2*D*), spleen (Fig. 2*E*), and heart (Fig. 2*F*), and was detected in mice that retained their implants, although this effect decreased over time, with bacteremia resolved by 1 d and spleen and heart infection undetectable by 14 dpi. In summary: (*i*) MRSA requires an implant to persistently colonize the UT; (*ii*) implants universally become colonized throughout a 2-wk infection; and (*iii*) dissemination into other organs can be detected as a sequela of CAUTI. The association with catheterization and rapid dissemination in this model is consistent with what has been reported for human MRSA UTI (4, 12), and suggests that catheterization alters the bladder environment, making it suitable for persistent MRSA UT colonization and dissemination.

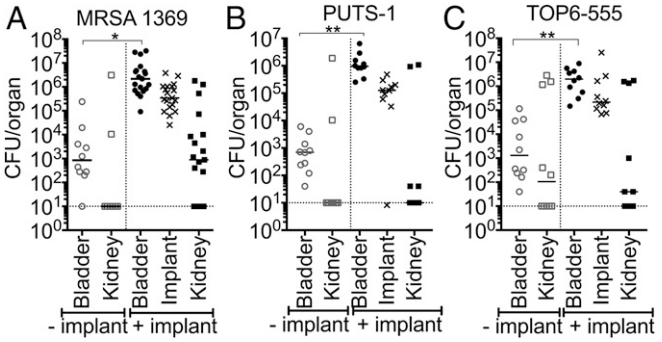

Fig. 1. Mouse model of *S. aureus* CAUTI. MRSA 1369 (*A*), PUTS-1 (*B*), and TOP6-555 (*C*) all require an implant to colonize bladders (circles) and kidneys (squares), and all implants (Xs) are colonized at 24 h post infection (hpi). Open and closed symbols denote nonimplanted mice and mice that retained the implant, respectively. Statistical significance was assessed using the Mann–Whitney *U* test, $*P < 0.01$, $**P < 0.001$.

MRSA Exacerbates the Inflammatory State of the Catheterized Bladder. Catheterization has been shown to induce a strong, localized inflammatory response that results in tissue damage and edema (26, 37, 38). Bladder inflammation in this model, measured via a change in bladder weight (37), was significantly increased in mock-infected implanted mice compared with naïve, as expected (naïve vs. PBS-I, 6 h; Fig. 3*A*). At early time points, inflammation in implanted mice was similar between infected and mock-infected mice (PBS-I vs. MRSA-I, 6 h; Fig. 3*A*). However, while inflammation in mock-infected mice remained relatively constant, inflammation continually increased in infected mice that retained the implant (1, 7, 14 dpi; Fig. 3*A*). By 14 dpi, infected bladder weights were significantly increased compared with implanted, mock-infected control mice or infected mice that lost the implant. Bladders with the highest weights developed abscesses (Fig. S2), and the implants recovered from these bladders were coated in thick puss-like exudations (Fig. S2*B*). Furthermore, the spleens

Downloaded at Palestinian Territory, occupied on December 15, 2021
www.manaraa.com

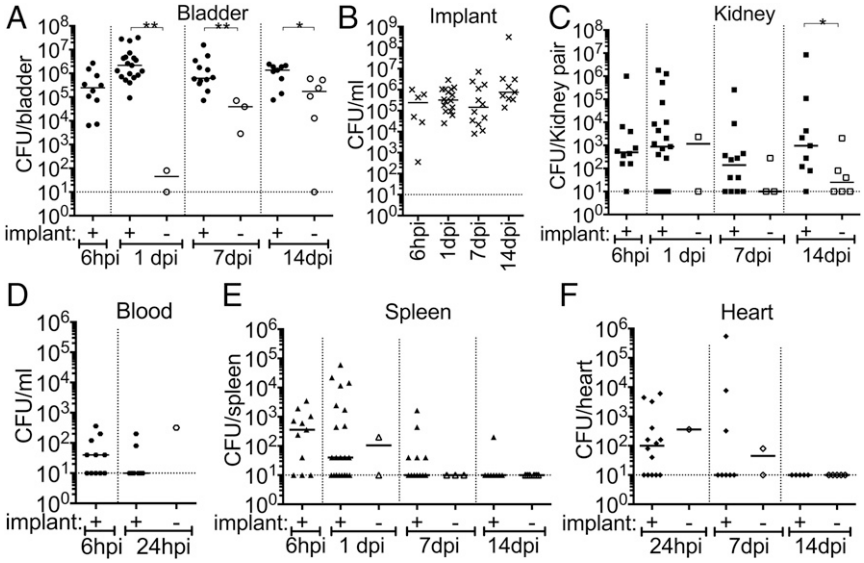

Fig. 2. Catheterization facilitates persistent, invasive MRSA CAUTI. (*A*) Mice with an implant maintain persistent bladder colonization. Mice that lose the implant display significantly lower bacterial burdens. (*B*) MRSA persistently colonizes the implant. (*C*) MRSA requires an implant to persistently colonize kidneys. (*D*) Bacteria were also detected in the blood at 6 h post implantation and infection (hpii), with most mice controlling the bacteremia by 1 dpii. (*E* and *F*) Mice also displayed dissemination to the spleen (*E*) and heart (*F*) at early time points but were able to control the disseminated infection by 14 dpii. Open and closed symbols denote mice that lost the implant and mice that retained the implant over the course of the experiment, respectively. Statistical significance was assessed using the Mann–Whitney *U* test, $*P < 0.05$, $**P < 0.005$.

from infected-implanted mice displayed significant splenomegaly (Fig. S3*A*), while the weights of kidneys (Fig. S3*B*) and hearts (Fig. S3*C*) remained similar between all mice. To gain insight into the impact of infection on the inflammatory response in implanted mice, bladder homogenates were used to assess the expression of a panel of cytokines. Of the 23 cytokines analyzed, 22 were induced >2-fold in infected implanted compared with noninfected implanted mice (Fig. 3 *B* and *C*), with 12 displaying >10-fold induction by 14 dpi (Fig. 3*C*). Together, these data indicated that persistent MRSA CAUTI exacerbates implant-induced inflammation and results in a highly inflamed state, which MRSA overcomes to cause disease.

Catheterization Creates a Permissive Environment for MRSA Urinary Tract Colonization. Catheterization induces the release of Fg in the bladders of both humans and mice (2, 26). Since it is well-established that Fg interactions promote MRSA pathogenesis in a diverse range of diseases (28–33), we hypothesized that Fg may play a key role in altering the UT environment to facilitate MRSA CAUTI. To test this, the presence and localization of Fg and MRSA were examined in the bladders of implanted-infected mice. Immunofluorescence staining revealed that in naïve mice Fg was not detected and the epithelium was intact (naïve, Fig. 4*A*). Staining for the presence of uroplakin III (UpIII), a crystalline protein matrix produced by the terminally differentiated umbrella cells of the bladder (26, 42), was used to delineate mucosal wounding. By 1 dpi in implanted mice, areas of the epithelia appeared compromised (1 dpi, Fig. 4*A*). Additionally, Fg was present in bladders (Fig. 4*A* and Fig. S4) and on catheters (Fig. 4*C*), and MRSA was found to colocalize with the deposited Fg. By 7 dpi, UpIII staining was diminished and cell nuclei staining became diffuse (7 dpi, Fig. 4*A*), which persisted through day 14 (14 dpi, Fig. 4*A*). The decreased UpIII staining is indicative of exfoliation of the umbrella cells, which was previously shown to be accompanied by an expansion of the proliferative zone (43). Additionally, an increase in Fg coating the underlying cells was observed, which likely aids in healing the damaged epithelium, and MRSA primarily colocalized with the accumulating Fg. At 14 d post implantation and infection, large aggregates of Fg formed in infected implanted bladders and MRSA was predominately found within these clumps (Fig. 4*B*). We next determined whether these findings translated to the clinic. Thus, we collected catheters from patients determined to have *S. aureus*-positive urine or catheter cultures (Table S2) to assess Fg and/or *S. aureus* deposition. We found that Fg was deposited on all patient catheters and *S. aureus* colocalized with deposited Fg (Fig. 5), despite receiving intensive antibiotic therapy (27) (Table S2). Together, these data indicate that Fg deposition on urinary catheters alters the UT environment, making it more suitable for MRSA adherence and persistent colonization.

Scanning Electron Microscopy of *S. aureus* Urinary Tract and Catheter Colonization. To more closely examine implants from mice and compare them with human urinary catheters, scanning electron microscopy (SEM) was used. Mice received implants and were either mock-infected or MRSA-infected for 24 h. Images of mock-infected implanted bladders revealed areas of epithelial cell damage (Fig. 6 *A* and *B*) and, in the latter, these areas were associated with large communities of MRSA, appearing similar to biofilms (Fig. 6 *B* and *C*). Immune cell infiltrates, likely neutrophils, were visible in the area surrounding MRSA, as well as encasing the bacteria (Fig. 6 *B* and *C*). Implants from both mock- and MRSA-infected mice had host cells and proteins associated with them (Fig. 6 *D* and *E*), which coincided with large communities of MRSA in infected mice (Fig. 6*E*). SEM analysis of catheters from human patients with *S. aureus*-positive cultures revealed similar features to mouse implants (Fig. 7*F*). Epithelial and immune cells, host proteins, consistent with Fg, and *S. aureus* were visible on the urinary catheters. These data suggest that our mouse model of MRSA CAUTI recapitulates aspects of human CAUTI where MRSA forms communities within the UT by incorporating host components, including Fg, that protect against clearance by immune cells and antibiotic therapy.

ClfA and ClfB Mutant Strains Display Expected Fibrinogen-Binding Phenotypes. ClfA and ClfB are two of the best-characterized members of the MSCRAMM family (32, 39, 40). Both adhesins are known to play critical roles in (*i*) binding to Fg; (*ii*) agglutination;

Downloaded at Palestinian Territory, occupied on December 15, 2021
www.manaraa.com

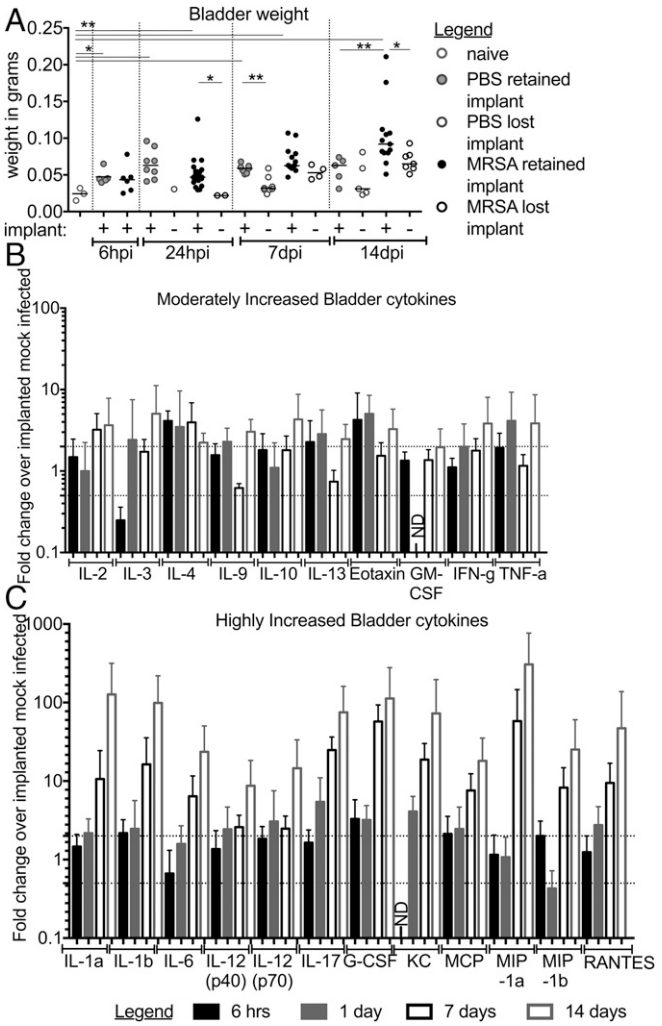

Fig. 3. MRSA CAUTI induces a localized inflammatory response. (*A*) Implants induce inflammation, which can be measured as an increase in bladder weight over time. Infection with MRSA 1369 following implantation further increases bladder inflammation. Light-gray circles represent naïve mice, dark-gray circles denote mock-infected implanted mice, and black circles are implanted-infected mice. Open circles denote mice that did not receive or that lost an implant, and closed circles represent mice that retained the implant over the course of the experiment. Statistical significance was assessed using the Mann–Whitney *U* test, $*P < 0.05$, $**P < 0.005$. (*B* and *C*) Cytokines increased >twofold (*B*) or >10-fold (*C*) in implanted MRSA-infected mice compared with implanted mock-infected control mice over a 2-wk time course. There are at least five independent data points represented in *B* and *C*. Error bars represent the mean with the standard deviation. ND, not determined.

and (*iii*) pathogenesis in diverse animal models (28, 29, 31–33, 39–41). Mutation of either gene results in decreased Fg binding and reduced virulence, albeit ClfA$^-$ strains typically display more striking phenotypes both in vitro and in vivo. Thus, to determine the role of MRSA–Fg interactions in the CAUTI model, we focused on characterizing *clfA*- and *clfB*-deficient mutants. To do this, transposon mutants in *clfA* and *clfB* (44, 45) were generated in MRSA 1369 creating strains ClfA$^-$ and ClfB$^-$, respectively (*SI Materials and Methods*). Both mutants had growth characteristics similar to WT in either rich media or human urine (Fig. S5). Next, these mutants were assessed for Fg-dependent agglutination and Fg adherence to confirm they displayed Fg-binding defects consistent with their published phenotypes (31, 40). For the Fg-dependent agglutination assay, the WT strain grown in either rich media (Fig. S6*A*) or urine (Fig. S6*B*) displayed significant agglutination upon the addition of Fg. Mutation in *clfA* significantly reduced this Fg-dependent agglutination by 57 to 70%, depending on the growth condition, as expected. Additionally, the ClfA$^-$ strain exhibited significantly reduced binding to Fg-coated wells compared with MRSA 1369 when grown in either rich media (Fig. S6*C*) or human urine (Fig. S6*D*). Consistent with previous reports (31, 33), the effect of the *clfB* mutation was more modest after growth in rich media, displaying a small but significant agglutination defect (~10% reduction) (Fig. S6*A*). However, after growth in human urine, the ClfB$^-$ strain's Fg-dependent agglutination defect was much more pronounced (~25% reduction) compared with WT (Fig. S6*B*). Paradoxically, while the *clfB* mutant displayed a significant reduction in binding to Fg-coated wells compared with WT after growth in rich media (Fig. S6*C*), consistent with previous reports (39), this reduction did not translate to ClfB binding to Fg-coated wells when the mutant was grown in urine (Fig. S6*D*). Finally, these strains were assessed for attachment to and colocalization with Fg on patient catheters (Fig. S6*E* and Table S2). Binding of the *clfA* and *clfB* mutants to the catheter was reduced compared with the WT strain, when grown in rich media (Fig. S6*E*). The residual binding that was observed was found to primarily colocalize with Fg on the catheter, likely due to the expression of at least ClfB in the *clfA* mutant or ClfA in the *clfB* mutant. Together, these data show that *clfA* and *clfB* mutants exhibited the expected in vitro phenotypes, indicating they play a role in binding and interacting with Fg. Additionally, the reported differential expression of *clfA* and *clfB* in vitro (46), together with these data, suggest ClfB–Fg interactions are sensitive to the growth conditions characteristic of the UT environment, implicating ClfB production as an important contributor to virulence.

ClfB Contributes to MRSA CAUTI. The contribution of ClfA and ClfB to CAUTI pathogenesis was then investigated by assessing the mutants in the mouse CAUTI model. Implanted mice were challenged with MRSA 1369 or the *clfA* or *clfB* mutants, and infection was evaluated by determining the CFUs recovered from bladders, implants, and kidneys. Despite its more pronounced phenotype in Fg interactions in vitro, the ClfA$^-$ strain was as proficient at causing CAUTI as the WT, with no significant differences in recovered CFUs at any of the sites tested at either day 1 (Fig. S7*A*) or day 3 (Fig. 7*A*). However, although it displayed less striking defects in Fg interactions compared with ClfA$^-$ in vitro, the ClfB$^-$ strain had a modest but significant reduction in bladder CFUs at day 1 (Fig. S7*B*). Furthermore, by day 3, the *clfB* mutant displayed an approximately 1 log defect in implant bacterial titers, which was significantly reduced compared with the WT (Fig. 7*B*). Together, these data establish that the loss of ClfB, but not ClfA, results in attenuation for CAUTI and suggests that ClfB–Fg interactions contribute to MRSA infection of the UT.

Discussion

While MRSA can grow readily in urine, suggesting that it can use the limited nutrients available in the UT habitat (42), paradoxically, it rarely causes uncomplicated UTI. It is, however, an emerging cause of complicated UTIs, including infected kidney stones (11, 47–49) and CAUTIs (4, 8, 9, 12, 21). Here we resolve this paradox by demonstrating that MRSA exploits the presence of Fg that is released as part of an inflammatory response induced by the presence of a foreign body. Elucidating the host factors that potentiate CAUTIs will be important for understanding patients' risk factors for developing severe sequelae.

Studies characterizing a mouse CAUTI model and human urinary catheterization indicate that even in the absence of infection, catheterization by itself induces a specific, localized inflammatory response due to mechanical damage caused by the

Downloaded at Palestinian Territory, occupied on December 15, 2021
www.manaraa.com

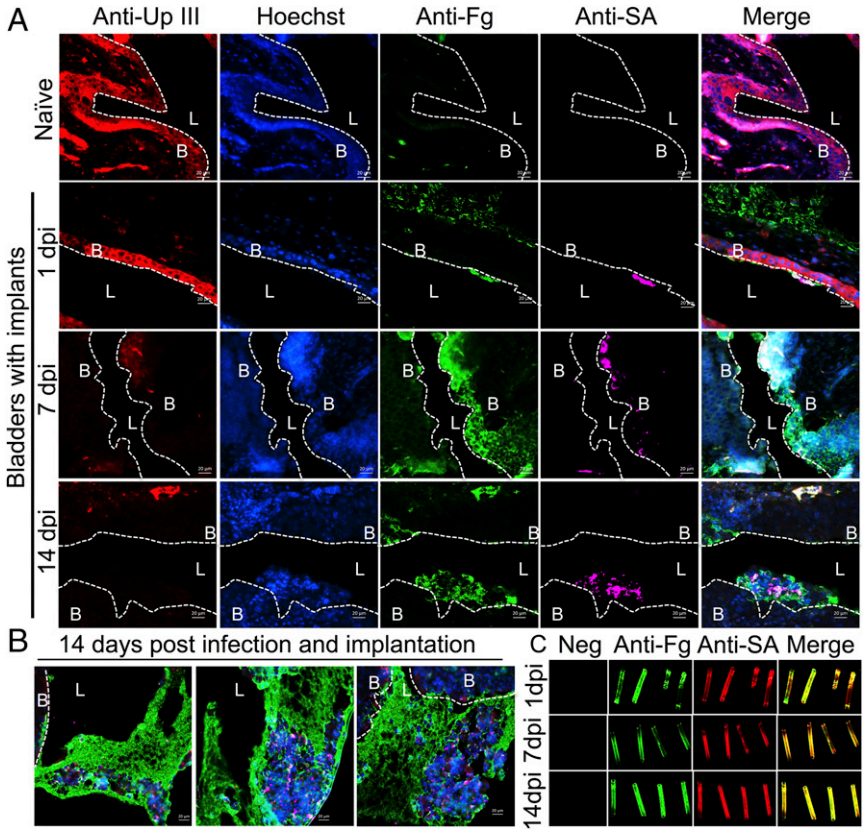

Fig. 4. Implants create a permissive environment for MRSA. (*A*) Representative images of a naïve mouse bladder or mouse bladders with implants at 1, 7, and 14 dpi. Sections were stained for uroplakin III (red), a protein that lines the umbrella cells of the bladder, cell nuclei (blue), fibrinogen (green), and MRSA (pink). Dotted white lines denote the separation of bladder tissue (B) from lumen (L). Infected mice with implants at day 1 have similar bladder morphology to naïve mice. However, by day 7, uroplakin III staining diminishes, while cell nuclei become smaller and staining becomes diffuse, which persists through day 14. This change in uroplakin III and cell nuclei staining is indicative of urothelial cell damage that results in exfoliation of the umbrella cells and an expansion of the underlying transitional layer. This, along with Fg coating the umbrella cells, is important for healing the damaged epithelium. However, MRSA predominately colocalizes with Fg accumulating on the epithelium, suggesting the protein plays a role in MRSA pathogenesis. (*B*) Representative images of mouse bladders at 14 d post infection and implantation. Large Fg aggregates form, encasing MRSA. (*C*) MRSA colocalizes with Fg deposited on implants at 1, 7, and 14 dpi. (Scale bars, 20 μm.)

catheter, which induces the release of host proteins, including Fg (26, 27, 36). In the mouse model, the proinflammatory profile upon catheterization was dominated by the up-regulation of IL-6, which is involved in the induction of Fg expression and potentiation of its release into the bladder lumen (26, 38, 50–52). Under normal circumstances, Fg is required to aid in the healing of damaged tissue (50, 52). In the mouse CAUTI model developed here, we found that MRSA exploits the deposition of Fg to mediate colonization of the bladder and catheter. Fg was only present in the bladder following the placement of an implant, as previously reported (26), and MRSA was found to primarily adhere to areas of the epithelium and implant that were coated with Fg. MRSA was also found to be associated with host epithelial cells and immune cell infiltrates on the mouse implants and human catheters. Further, MRSA infection promoted a robust inflammatory response in the presence of an implant, resulting in up-regulation of numerous proinflammatory cytokines, leading to highly inflamed and abscessed bladders. Specifically, in long-term implanted/infected mice, cytokines known to play additional roles in signaling the release of Fg (50–52), including IL-1α, IL-1β, IL-6, and TNF-α (tumor necrosis factor α), were all up-regulated. This correlated with the presence of large aggregates of Fg that were only observed in long-term implanted/infected bladders, suggesting the placement of an implant and infection induced a synergistic effect, which promoted more pronounced Fg accumulation. Importantly, MRSA was primarily found within the Fg agglutinates. The abundance of Fg as part of the host's response to foreign bodies suggests that Fg is a critical component of MRSA pathogenesis, which is supported by the observation that MRSA also preferentially bound to Fg-coated regions of urinary catheters from human patients.

Interactions between MRSA and Fg are known to contribute to pathogenesis in other models of disease, including central line infections and animal models of systemic infection and endocarditis, and have, therefore, been the subject of considerable investigation (28, 29, 31–33, 40, 53, 54). Specifically, Fg deposition on human venous catheters has long been recognized as an essential step in MRSA attachment and persistence in central line infections (54). Direct contact with blood and platelets, which are full of Fg, causes the venous catheters to immediately become coated following placement (29, 54, 55). MRSA exploits the presence of Fg for attachment and the formation of communities that protect against the host immune system (29, 53–55). Additionally, an important step in MRSA pathogenesis in systemic infection is abscess formation, which is dependent on the formation of a fibrin pseudocapsule around the bacteria (53). In this model, MRSA is initially introduced directly into the bloodstream and subsequently disseminates to organ tissues. Once in the organ tissue, MRSA elicits a robust immune response, which results in the destruction of the tissue. Fg and fibrin are then deposited in the tissue, which MRSA exploits to form a fibrin pseudocapsule. This pseudocapsule allows bacterial replication and protects against clearance by the massive influx of immune cells recruited

Downloaded at Palestinian Territory, occupied on December 15, 2021
www.manaraa.com

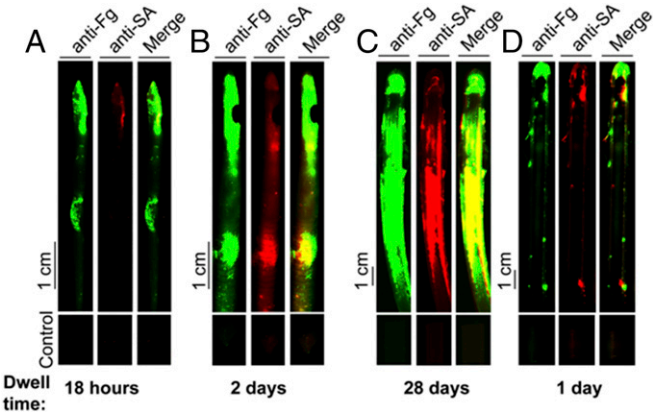

Fig. 5. *S. aureus* colocalizes with Fg deposited on patients' catheters. Immunofluorescence staining of catheters 6 (*A*), 12 (*B*), 57 (*C*), and 64 (*D*) (Table S2) from patients with *S. aureus* urine or catheter positive cultures indicates Fg was deposited and, despite receiving appropriate antibiotic treatment, *S. aureus* was found on all catheters colocalizing with deposited Fg.

in response to the pathogen. Abscess maturation relies on the formation of zones of necrotic and healthy immune cells, which are thought to contribute to the further destruction of host tissue, releasing nutrients required for bacterial survival and allowing for bacterial escape from the abscess to undergo additional rounds of infection. Together, these data strongly suggest that MRSA uses similar mechanisms of pathogenesis for venous and urinary catheter infection and systemic disease, where Fg deposition alters the surface of the catheter and epithelium to promote staphylococcal adherence and the formation of communities to resist clearance.

Several factors responsible for promoting MRSA–Fg interactions have been characterized, including the two MSCRAMMs ClfA and ClfB (32, 39, 40). Mutants deficient for ClfA typically display striking in vitro defects in interacting with Fg and are severely attenuated for pathogenesis in models of systemic infection and endocarditis (31, 32, 39, 40). In contrast, the closely related ClfB MSCRAMM displays more modest Fg interaction defects in vitro and virulence defects in models of systemic infection (28, 40). Consistent with previous reports for other strains (31, 32, 39, 40), the loss of ClfA in MRSA 1369 resulted in more prominent defects for Fg-dependent agglutination and adherence compared with ClfB. However, in the mouse CAUTI model, the loss of ClfA had no observable impact on MRSA pathogenesis. In contrast, the loss of ClfB resulted in attenuation compared with MRSA 1369. While the molecular basis of this discrepancy is unknown, it has been established that while the two proteins exhibit highly similar structural organization, there are significant differences in how they interact with Fg. For example, ClfA and ClfB recognize distinct sites on Fg: ClfA binds the C-terminal γ-chain of Fg, while ClfB recognizes the Fg α-chain (56). Additionally, the differences in the ClfA and ClfB phenotypes may be explained by the observed difference in the adhesins' expression in vitro, as ClfA is expressed at all phases of growth whereas ClfB is only expressed in the early exponential phase during aerobic growth (40, 46). Differences in regulation could explain the relative importance of ClfB in the bladder habitat. Consistent with this hypothesis, we observed that the relative contributions of ClfA and ClfB to Fg binding differed between cultures grown in rich media vs. those grown in human urine. These differences also demonstrate that Fg-binding behavior under standard in vitro conditions may not always be predictive of expression patterns induced upon encountering in vivo environments. These data also support the long-held hypothesis that MRSA encodes several potentially redundant Fg-binding proteins because they play unique roles in different types of infections or host compartments. Thus, understanding how the host environment influences interactions with Fg will be important for understanding the unique challenges the UT habitat presents to MRSA pathogenesis.

Our previous reports show that *E. faecalis* shares several common features with MRSA during CAUTI (26, 36–38, 57). First, both *E. faecalis* and MRSA cause persistent disease by overcoming the inflammation induced upon implant placement, which consists of the recruitment of immune cells, including activated macrophages and neutrophils (37). Additionally, both pathogens exacerbate the implant-induced inflammation by up-regulating additional cytokines known to signal neutrophil activation or recruitment, including IL-17, IL1-β, granulocyte colony-stimulating factor, and keratinocyte-derived chemokine (58–60) and, during *E. faecalis* infection, correlated with increased numbers of activated neutrophils within the implanted bladder (37). Additionally, both pathogens up-regulate expression of IL-6 following infection above the levels induced by the implant alone (37). *E. faecalis* also exploits the presence of Fg to form biofilm on catheter implants during CAUTI (26). Induction of IL-6 following implant placement correlates with increased Fg in the bladder. The observed increase of IL-6 and accumulation of Fg after MRSA and *E. faecalis* infection suggest both pathogens (*i*) use a common mechanism for release and accumulation of Fg and (*ii*) exploit Fg to promote attachment and biofilm formation during CAUTI. Additionally, *E. faecalis* forms essential interactions with Fg via the pilus tip protein EbpA, which has several features in common with MRSA's ClfB. The ClfB crystal structure has been solved, and molecular modeling of EbpA suggests the protein shares a similar structural organization and maintains an analogous central Fg-binding groove to ClfB (46, 57, 61). Additionally, both ClfB and EbpA contain a metal ion-dependent adhesion-site motif, which in ClfB, and likely in EbpA, binds metal cations and coordinates the Fg-binding groove facilitating ligand binding (46, 61). The similarities between these proteins and the fact that both contribute to CAUTI pathogenesis suggest that staphylococci and enterococci likely use a general mechanism of pathogenesis by exploiting the accumulation of Fg to initiate catheter-related infections.

Despite these similarities, there are several important differences *E. faecalis* and MRSA use to establish persistent CAUTI. *E. faecalis* tightly regulates the inflammatory response by primarily inducing IL-6 to promote additional release of Fg (26, 37, 38). The limited induction of other inflammatory cytokines during *E. faecalis* infection moderates inflammatory-mediated damage to the bladder tissue (26, 36). The specific and controlled release of Fg during implant placement allows *E. faecalis* to establish long-term, relatively "quiet" persistent infection. In contrast, MRSA's preference for abscess formation (53) results in the induction of a robust inflammatory response, specifically recruiting immune cells and up-regulating multiple pathways for Fg induction. In this highly inflamed state of a persistent MRSA CAUTI in the mouse model, spleens become enlarged and abscesses form in the bladder. Not surprisingly, MRSA up-regulates many more cytokines than *E. faecalis* that are involved in the recruitment and activation of neutrophils, including MIP-1α and β, RANTES, TNF-α, and IFN-γ (58–60). These cytokines likely contribute to the unique aspects of MRSA vs. *E. faecalis* CAUTI, including the massive influx of neutrophils that become associated with MRSA, abscess formation, the "puss-like" exudates coating the catheter, and increased destruction of tissue, which were revealed by SEM analysis of infected-implanted bladders. The SEM analysis also indicated that MRSA forms biofilm-like communities on the implants that incorporated host components, including Fg, which can explain how MRSA can resist this immune onslaught and persist in patient bladders despite rigorous antibiotic treatment. Overall, the up-regulation of IL-6, IL-10, TNF-α, IFN-γ, IL1-β, and IL-4 and

Downloaded at Palestinian Territory, occupied on December 15, 2021
www.manaraa.com

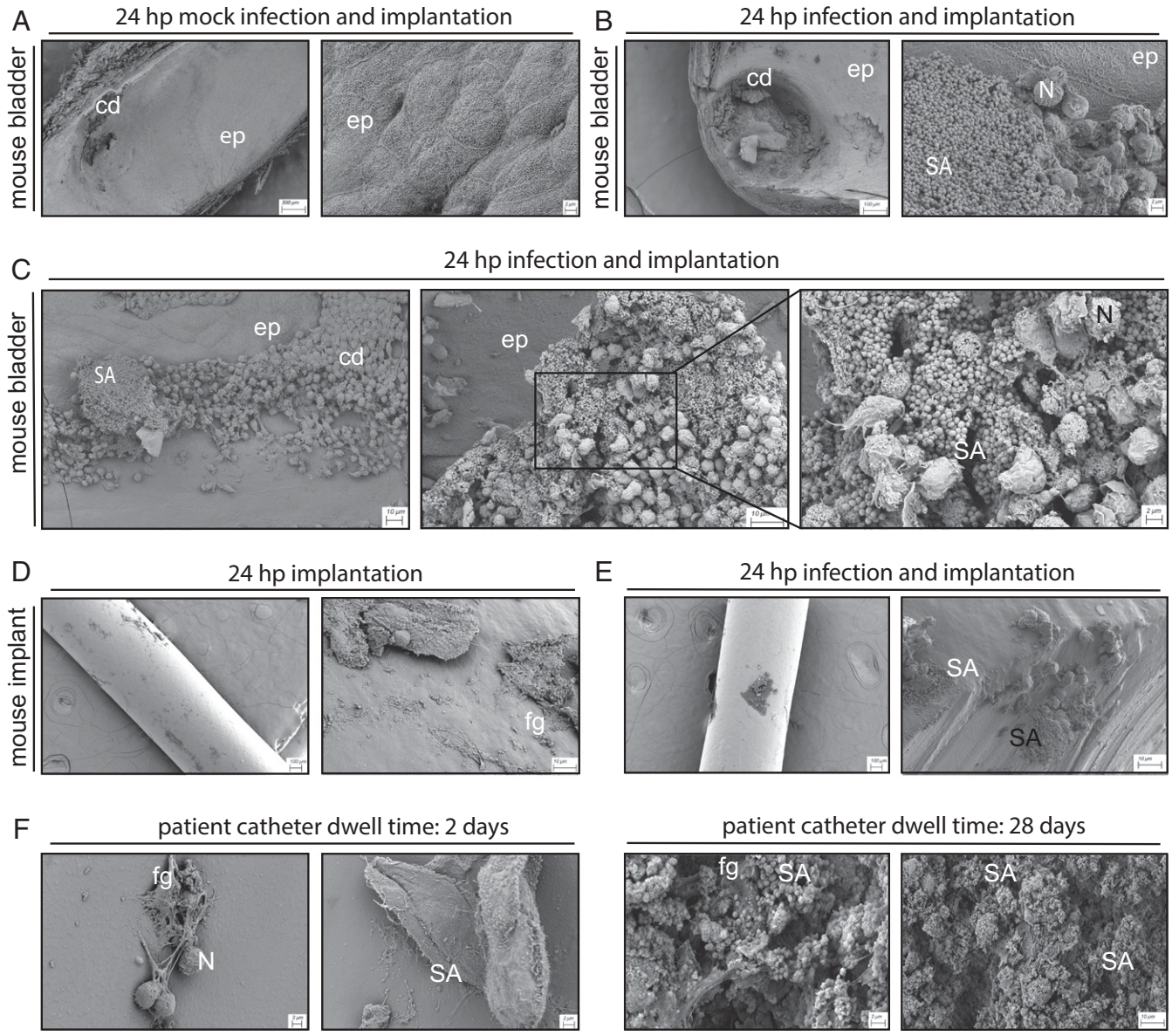

Fig. 6. Representative SEM images of mouse bladders, implants, and human catheters. Tissues, implants, and catheters were processed following implantation, implantation and infection (mouse), or dwell time (human). (*A–C*) Mouse bladders, with each pair showing low-, medium-, and (*C*) high-magnification images as indicated. (Scale bars: 200, 100, and 2 μm, respectively.) (*D* and *E*) Implants, with each pair showing medium- and high-magnification images, as indicated. (Scale bars: 100 and 10 μm, respectively.) Three mice were used per group. (*F*) Human catheters, with each pair showing two representative images from catheters recovered from the patients analyzed in Fig. 5. [Scale bars: 2 and 10 μm (*Far Right*).] Labeled are the epithelium (ep); epithelial cell damage from the implant (cd); MRSA (SA); immune cell infiltrates, likely neutrophils (N); and proteins, likely fibrinogen (fg).

concurrent infiltration of activated neutrophils in this CAUTI model are consistent with other models of *S. aureus* infection, as the recruitment and activation of immune cell infiltrates, including neutrophils, are a hallmark of human blood infection, skin and soft tissue infection, and systemic disease (53, 59, 62, 63). These data suggest that while MRSA and *E. faecalis* both exploit the host's inflammatory response to cause CAUTI, they pursue fundamentally different mechanisms to resist the immune system and establish persistent disease.

The Infectious Diseases Society of America recently described the "ESKAPE" pathogens as a cohort of bacterial species that are now the most adept at escaping the actions of antibiotics (64). Significantly, this group includes the staphylococci and enterococci along with several others that are major causes of hospital-associated infections (HAIs). By elucidating the mechanisms of CAUTI pathogenesis, the results of the present study may provide important insights for developing more effective therapies for the treatment of HAIs. Further characterization of foreign-body models will give insight into how the host environment or the surface of implanted devices is altered following placement and the inflammatory response that is induced. The deposition of other host matrix proteins, including fibronectin and elastin, on prostheses is known to promote bacterial adhesion and facilitate persistent infection (39). Here we also show that *S. aureus* (*i*) exploits Fg deposition during a mouse CAUTI model via ClfB interactions and (*ii*) specifically colocalizes with Fg deposited on catheters from patients with *S. aureus*-positive cultures, despite the patients receiving appropriate, intensive antibiotic therapy (27). This suggests that an approach that can disrupt or prevent interaction with Fg may be developed as an

Downloaded at Palestinian Territory, occupied on December 15, 2021
www.manaraa.com

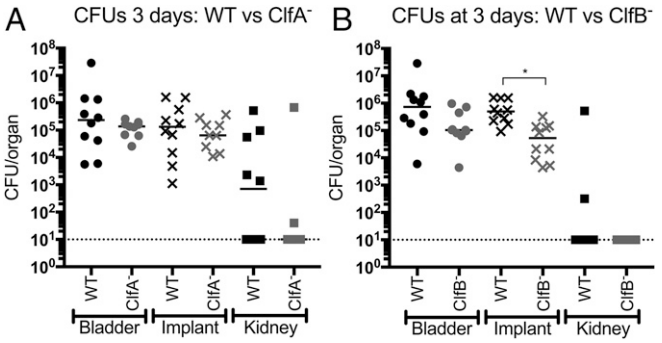

Fig. 7. Fg-binding protein ClfB, but not ClfA, contributes to CAUTI. (*A*) The *clfA* mutant displayed similar bladder, implant, and kidney burdens to the wild type. (*B*) ClfB^{-} exhibited significantly reduced bacterial titers on the implant at day 3 compared with WT. Statistical analysis was performed using the Mann–Whitney *U* test, $^{*}P < 0.005$.

antibiotic-sparing therapy. Such therapies may be broadly effective, as MRSA–Fg interactions are an important step in MRSA pathogenesis, including Fg coating of venous catheters and other biomaterials and fibrin pseudocapsule formation during abscess community maturation (29, 39, 53, 55). Detailed investigation of the immune response elicited by foreign bodies and other potential proteins deposited on medical devices that promote staphylococcal infection will be essential for fully understanding MRSA pathogenesis to develop effective therapeutics. The availability of animal models like the MRSA CAUTI model developed here should prove invaluable for understanding the pathogenesis of important HAIs caused by ESKAPE pathogens.

Materials and Methods

Bacterial Strains and Growth Conditions. All strains used in this study are shown in Table S1, all primers used in this study are listed in Table S3 and detailed protocols are described in *SI Materials and Methods*).

Growth Assays. Bacteria from overnight cultures were subcultured in either pooled, filter-sterilized human female urine at pH 5.0, 6.0, or 7.0 or brain heart infusion (BHI) to a starting OD_{600} of 0.02. Bacterial growth was measured approximately every 45 min for 24 h via an Epoch (BioTek) microplate spectrophotometer. At least three separate experiments were performed with five wells per experiment for each strain.

Mouse Model of Catheter-Associated UTI and CFU Enumeration. C57BL/6 female mice were transurethrally implanted with a small piece of silicone tubing (catheter implant) and inoculated as previously described (38). Briefly, mice were infected immediately following implant placement with $\sim 2 \times 10^7$ CFUs of bacteria transurethrally. Organs and implants were harvested and weighed at the indicated time points and the bacterial load was determined (see *SI Materials and Methods* for more details). Statistical analyses were performed using the Mann–Whitney *U* test with GraphPad Prism software (version 6.0 for Mac). All animal studies were performed in accordance with the guidelines of the Committee for Animal Studies at Washington University School of Medicine.

Cytokine Profiling. Bladder homogenates from mock-infected or MRSA 1369-infected implanted mice for 6 h, 1 d, 7 d, and 14 d were frozen at −80 °C until time of assay. Before cytokine analysis, homogenates were thawed on ice and microcentrifuged at 11,000 × *g* for 10 min, and supernates were transferred to a new tube. Cytokine expression in supernates was then assessed using the Bio-Plex 23-Plex Assay Kit from Bio-Rad Laboratories following the manufacturer's protocols.

Antibodies Used in This Study. Primary antibodies used were goat anti-fibrinogen (Sigma-Aldrich); mouse anti-uroplakin III (Research Diagnostics); and rabbit anti-protein A (Sigma-Aldrich). Secondary antibodies used were Alexa Fluor 488-labeled donkey anti-goat, Alexa Fluor 594-labeled donkey anti-mouse, Alexa Fluor 647-labeled donkey anti-rabbit, IRDye 800CW donkey anti-goat, and IRDye 680LT goat anti-rabbit. Alexa Fluor antibodies were purchased from Invitrogen Molecular Probes, and IRDye conjugate antibodies were purchased from LI-COR Biosciences.

Immunohistochemistry and Histopathology. Mouse bladders were fixed in formalin overnight at 4 °C and implants were fixed for 1 to 2 h at room temperature and processed for immunofluorescence staining as previously described (26). Implants were washed and kept at 4 °C until immunostaining was performed. Bladders were processed and sectioned for staining (see *SI Materials and Methods* for more details). Sections were blocked, washed, and incubated with primary antibodies and then secondary antibodies, and washed again. Last, sections were counterstained with Hoechst dye specific for DNA. A Zeiss Axioskop 2 MOT Plus microscope was used to analyze the sections via epifluorescence microscopy. Implants were blocked, washed, and incubated with primary and then Odyssey secondary IRDye 800CW and IRDye 680LT antibodies (see *SI Materials and Methods* for more details). Last, implants were washed and allowed to air dry. The Odyssey Imaging System (LI-COR Biosciences) was used to examine the infrared signal. Controls for autofluorescence included nonimplanted catheters.

Collection of Human Urinary Catheters. To investigate whether Fg or *S. aureus* could be detected on human urinary catheters, patients 18 y or older in the Urology Department at Washington University School of Medicine undergoing catheterization were consented and enrolled in our study. The dwell time, urine culture, and antibiotics prescribed were recorded for each patient (Table S2) as previously published (27). The Washington University School of Medicine Internal Review Board approved this study (approval 210410058) (see *SI Materials and Methods* for more details on each catheter used in this study).

Analysis of Human Urinary Catheters. Following collection, catheters were processed as previously described (27). Briefly, the first 10 cm of the catheter's tip was blocked, washed, and incubated with primary and then Odyssey secondary IRDye 800CW and IRDye 680LT antibodies (see *SI Materials and Methods* for more details). The Odyssey Imaging System (LI-COR Biosciences) was used to examine the infrared signal. Images were analyzed using Odyssey Infrared Imaging software (version 3.0.16) to determine the infrared fluorescence at 800 nm (Fg) and 700 nm (*S. aureus*). Controls for autofluorescence included nonimplanted catheters and catheters not incubated with the primary antibodies.

Scanning Electron Microscopy of Bladders and Catheters. Mouse bladders, 1-d post implantation and mock- or MRSA-infected, were prepared by the "balloon method" and imaged by field emission-scanning electron microscope (FE-SEM) (Zeiss Merlin equipped with a Gemini II electron column) (see *SI Materials and Methods* for detailed methods). Unstained, fixed sections of human urinary catheters from patients with *S. aureus*-positive cultures (Table S2, catheters 12 and 57) were selected and processed for SEM as described in *SI Materials and Methods*.

Agglutination Assay. To determine whether ClfA^{-} and ClfB^{-} strains displayed Fg-binding defects, agglutination assays were performed as previously described (33). Briefly, bacterial strains grown overnight under shaking conditions (200 rpm) at 37 °C were subcultured and grown to an OD_{600} of 1.0. Strains were washed and resuspended in one volume of 1× PBS. Human Fg (FIB 3; Enzyme Research Laboratories) was added to a final concentration of 250 μg/mL or, as a negative control, an equivalent amount of PBS. One hundred-microliter aliquots of supernatant were then removed and OD_{600} was measured via an Epoch (BioTek) microplate spectrophotometer every hour until the supernatant cleared. Agglutination was calculated using the following formula: percentage agglutination = $[(OD_{time0} - OD_{timeT})/OD_{time0}] \times 100$.

Whole-Bacteria Binding to Fibrinogen. To assess whether MRSA strains could adhere to immobilized Fg, microplates were coated with 100 μg/mL human Fg, as previously described (26). Briefly, bacterial strains were grown overnight in BHI or human urine and normalized to an OD_{600} of 0.5. A total of 100 μL bacteria was added to the Fg-coated wells, incubated for 1 h, and then washed to remove all unbound bacteria. The plates were incubated with primary and then Odyssey secondary IRDye 680 LT antibody (see *SI Materials and Methods* for more details). Infrared signal was detected by scanning the plates using the Odyssey Imaging System (LI-COR Biosciences), and intensity was calculated via Image Studio software (LI-COR Biosciences).

Ex Vivo Attachment to Human Urinary Catheters. Catheters from patients with negative urine cultures (Table S2) were selected to determine whether ClfA^{-}

Downloaded at Palestinian Territory, occupied on December 15, 2021
www.manaraa.com

or ClfB$^-$ strains were required for binding, as previously described (27). Briefly, overnight cultures were washed and resuspended in PBS. Two centimeters of the fixed catheter tip was incubated with ~1×10^7 CFUs of each bacterial strain or PBS alone for 1 h. Catheters were washed to remove all unbound bacteria, fixed for 20 min, washed again, and blocked. Catheters were washed and stained with primary antibody and then Odyssey secondary IRDye 800CW and IRDye 680LT antibodies and assessed for infrared signal via the Odyssey Imaging System (see *SI Materials and Methods* for more details).

Statistical Analyses. Data from multiple experiments were pooled for each assay. The mean and SD were calculated for all growth assays using Prism 6 and 7 software (GraphPad Software). For all CAUTI experiment comparisons, two-tailed Mann–Whitney *U* tests were performed using GraphPad Prism 6 and 7 software. Agglutination and whole-bacteria binding assays were analyzed by the Student's *t* test to evaluate statistical differences using GraphPad Prism 7 software.

ACKNOWLEDGMENTS. We thank Dr. Stephanie Fritz for providing the SSTI-MRSA and Co-MRSA strains; Dr. Anne Stapleton for providing the PUTS-1 4-147 strain; BEI Resources for providing the Nebraska Transposon Mutant Library (NR-48501), from which we obtained the *clfA* and *clfB* transposon mutants used in this study; and our clinical coordinator, Aleksandra Klim, and the urology team. This work was supported by Grants R01-DK051406 and R01-AI108749-01 (to J.N.W., A.L.F.-M., C.L.P., H.L.S., J.S.P., M.G.C., and S.J.H.) from the National Institute of Diabetes and Digestive and Kidney Diseases and National Institute of Allergy and Infectious Diseases, Grant 1F32DK104516-01 (to A.L.F.-M.), Monsanto Graduate Excellence Fund (H.L.S.), Children's Discovery Institute of Washington University and St. Louis Children's Hospital (CDI-CORE-2015-505) (to M.S.J. and J.A.J.F.), and the Foundation for Barnes-Jewish Hospital (3770).

1. Barrett SP, et al. (1999) Antibiotic sensitivity of bacteria associated with community-acquired urinary tract infection in Britain. *J Antimicrob Chemother* 44:359–365.
2. Flores-Mireles AL, Walker JN, Caparon M, Hultgren SJ (2015) Urinary tract infections: Epidemiology, mechanisms of infection and treatment options. *Nat Rev Microbiol* 13: 269–284.
3. Zhanel GG, et al.; NAUTICA Group (2005) Antibiotic resistance in outpatient urinary isolates: Final *results* from the North American Urinary Tract Infection Collaborative Alliance (NAUTICA). *Int J Antimicrob Agents* 26:380–388.
4. Al Mohajer M, Musher DM, Minard CG, Darouiche RO (2013) Clinical significance of *Staphylococcus aureus* bacteriuria at a tertiary care hospital. *Scand J Infect Dis* 45: 688–695.
5. Gilbert NM, et al. (2013) Urinary tract infection as a preventable cause of pregnancy complications: Opportunities, challenges, and a global call to action. *Glob Adv Health Med* 2:59–69.
6. Mylotte JM, Tayara A, Goodnough S (2002) Epidemiology of bloodstream infection in nursing home residents: Evaluation in a large cohort from multiple homes. *Clin Infect Dis* 35:1484–1490.
7. Naimi TS, et al. (2003) Comparison of community- and health care-associated methicillin-resistant *Staphylococcus aureus* infection. *JAMA* 290:2976–2984.
8. Routh JC, Alt AL, Ashley RA, Kramer SA, Boyce TG (2009) Increasing prevalence and associated risk factors for methicillin resistant *Staphylococcus aureus* bacteriuria. *J Urol* 181:1694–1698.
9. Saidel-Odes L, Riesenberg K, Schlaeffer F, Borer A (2009) Epidemiological and clinical characteristics of methicillin sensitive *Staphylococcus aureus* (MSSA) bacteriuria. *J Infect* 58:119–122.
10. Sharma I, Paul D (2012) Prevalence of community acquired urinary tract infections in Silchar Medical College, Assam, India and its antimicrobial susceptibility profile. *Indian J Med Sci* 66:273–279.
11. Bichler KH, et al. (2002) Urinary infection stones. *Int J Antimicrob Agents* 19:488–498.
12. Muder RR, et al. (2006) Isolation of *Staphylococcus aureus* from the urinary tract: Association of isolation with symptomatic urinary tract infection and subsequent staphylococcal bacteremia. *Clin Infect Dis* 42:46–50.
13. Muder RR, Brennen C, Wagener MM, Goetz AM (1992) Bacteremia in a long-term-care facility: A five-year prospective study of 163 consecutive episodes. *Clin Infect Dis* 14:647–654.
14. Ghenghesh KS, et al. (2009) Uropathogens from diabetic patients in Libya: Virulence factors and phylogenetic groups of *Escherichia coli* isolates. *J Med Microbiol* 58: 1006–1014.
15. Lachant DJ, Apostolakos M, Pietropaoli A (2013) Methicillin resistant *Staphylococcus aureus* prostatic abscess with bacteremia. *Case Rep Infect Dis* 2013:613961.
16. Ackermann RJ, Monroe PW (1996) Bacteremic urinary tract infection in older people. *J Am Geriatr Soc* 44:927–933.
17. Huggan PJ, Murdoch DR, Gallagher K, Chambers ST (2008) Concomitant *Staphylococcus aureus* bacteriuria is associated with poor clinical outcome in adults with *S. aureus* bacteraemia. *J Hosp Infect* 69:345–349.
18. Shigemura K, et al. (2013) Clinical factors associated with shock in bacteremic UTI. *Int Urol Nephrol* 45:653–657.
19. Gupta K, Bhadelia N (2014) Management of urinary tract infections from multidrug-resistant organisms. *Infect Dis Clin North Am* 28:49–59.
20. Pendleton JN, Gorman SP, Gilmore BF (2013) Clinical relevance of the ESKAPE pathogens. *Expert Rev Anti Infect Ther* 11:297–308.
21. Baraboutis IG, et al. (2010) Primary *Staphylococcus aureus* urinary tract infection: The role of undetected hematogenous seeding of the urinary tract. *Eur J Clin Microbiol Infect Dis* 29:1095–1101.
22. Cope M, et al. (2009) Inappropriate treatment of catheter-associated asymptomatic bacteriuria in a tertiary care hospital. *Clin Infect Dis* 48:1182–1188.
23. Trautner BW, Darouiche RO (2004) Catheter-associated infections: Pathogenesis affects prevention. *Arch Intern Med* 164:842–850.
24. Federspiel JJ, Stearns SC, Peppercorn AF, Chu VH, Fowler VG, Jr (2012) Increasing US rates of endocarditis with *Staphylococcus aureus*: 1999–2008. *Arch Intern Med* 172: 363–365.
25. DeLeo FR, Chambers HF (2009) Reemergence of antibiotic-resistant *Staphylococcus aureus* in the genomics era. *J Clin Invest* 119:2464–2474.
26. Flores-Mireles AL, Pinkner JS, Caparon MG, Hultgren SJ (2014) EbpA vaccine antibodies block binding of *Enterococcus faecalis* to fibrinogen to prevent catheter-associated bladder infection in mice. *Sci Transl Med* 6:254ra127.
27. Flores-Mireles AL, et al. (2016) Fibrinogen release and deposition on urinary catheters placed during urological procedures. *J Urol* 196:416–421.
28. Cheng AG, et al. (2009) Genetic requirements for *Staphylococcus aureus* abscess formation and persistence in host tissues. *FASEB J* 23:3393–3404.
29. Cheung AL, Fischetti VA (1990) The role of fibrinogen in staphylococcal adherence to catheters in vitro. *J Infect Dis* 161:1177–1186.
30. Kapral FA (1966) Clumping of *Staphylococcus aureus* in the peritoneal cavity of mice. *J Bacteriol* 92:1188–1195.
31. McAdow M, et al. (2011) Preventing *Staphylococcus aureus* sepsis through the inhibition of its agglutination in blood. *PLoS Pathog* 7:e1002307.
32. Rivera J, Vannakambadi G, Höök M, Speziale P (2007) Fibrinogen-binding proteins of gram-positive bacteria. *Thromb Haemost* 98:503–511.
33. Walker JN, et al. (2013) The *Staphylococcus aureus* ArlRS two-component system is a novel regulator of agglutination and pathogenesis. *PLoS Pathog* 9:e1003819.
34. Rothfork JM, Dessus-Babus S, Van Wamel WJ, Cheung AL, Gresham HD (2003) Fibrinogen depletion attenuates *Staphyloccocus aureus* infection by preventing density-dependent virulence gene up-regulation. *J Immunol* 171:5389–5395.
35. Cardile AP, et al. (2014) Human plasma enhances the expression of staphylococcal microbial surface components recognizing adhesive matrix molecules promoting biofilm formation and increases antimicrobial tolerance in vitro. *BMC Res Notes* 7:457.
36. Flores-Mireles AL, et al. (2016) Antibody-based therapy for enterococcal catheter-associated urinary tract infections. *MBio* 7:e01653-16.
37. Guiton PS, Hannan TJ, Ford B, Caparon MG, Hultgren SJ (2013) *Enterococcus faecalis* overcomes foreign body-mediated inflammation to establish urinary tract infections. *Infect Immun* 81:329–339.
38. Guiton PS, Hung CS, Hancock LE, Caparon MG, Hultgren SJ (2010) Enterococcal biofilm formation and virulence in an optimized murine model of foreign body-associated urinary tract infections. *Infect Immun* 78:4166–4175.
39. Arciola CR, et al. (2011) Concise survey of *Staphylococcus aureus* virulence factors that promote adhesion and damage to peri-implant tissues. *Int J Artif Organs* 34:771–780.
40. Foster TJ, Höök M (1998) Surface protein adhesins of *Staphylococcus aureus*. *Trends Microbiol* 6:484–488.
41. Roche FM, et al. (2003) Characterization of novel LPXTG-containing proteins of *Staphylococcus aureus* identified from genome sequences. *Microbiology* 149: 643–654.
42. Wright KJ, Hultgren SJ (2006) Sticky fibers and uropathogenesis: Bacterial adhesins in the urinary tract. *Future Microbiol* 1:75–87.
43. O'Brien VP, et al. (2016) A mucosal imprint left by prior *Escherichia coli* bladder infection sensitizes to recurrent disease. *Nat Microbiol* 2:16196.
44. Bae T, Glass EM, Schneewind O, Missiakas D (2008) Generating a collection of insertion mutations in the *Staphylococcus aureus* genome using bursa aurealis. *Methods Mol Biol* 416:103–116.
45. Fey PD, et al. (2013) A genetic resource for rapid and comprehensive phenotype screening of nonessential *Staphylococcus aureus* genes. *MBio* 4:e00537-12.
46. Ní Eidhin D, et al. (1998) Clumping factor B (ClfB), a new surface-located fibrinogen-binding adhesin of *Staphylococcus aureus*. *Mol Microbiol* 30:245–257.
47. Flannigan R, Choy WH, Chew B, Lange D (2014) Renal struvite stones—Pathogenesis, microbiology, and management strategies. *Nat Rev Urol* 11:333–341.
48. Hedelin H (2002) Uropathogens and urinary tract concretion formation and catheter encrustations. *Int J Antimicrob Agents* 19:484–487.
49. Paonessa JE, Gnessin E, Bhojani N, Williams JC, Jr, Lingeman JE (2016) Preoperative bladder urine culture as a predictor of intraoperative stone culture results: Clinical implications and relationship to stone composition. *J Urol* 196:769–774.
50. Jennewein C, et al. (2011) Novel aspects of fibrin(ogen) fragments during inflammation. *Mol Med* 17:568–573.
51. Zandbergen F, Plutzky J (2007) PPARalpha in atherosclerosis and inflammation. *Biochim Biophys Acta* 1771:972–982.
52. Sörensen-Zender I, et al. (2013) Role of fibrinogen in acute ischemic kidney injury. *Am J Physiol Renal Physiol* 305:F777–F785.
53. Cheng AG, DeDent AC, Schneewind O, Missiakas D (2011) A play in four acts: *Staphylococcus aureus* abscess formation. *Trends Microbiol* 19:225–232.
54. François P, Vaudaux P, Lew PD (1998) Role of plasma and extracellular matrix proteins in the physiopathology of foreign body infections. *Ann Vasc Surg* 12:34–40.
55. Cheung AL, Fischetti VA (1989) Role of surface proteins in staphylococcal adherence to fibers in vitro. *J Clin Invest* 83:2041–2049.

PNAS PLUS
MICROBIOLOGY
Downloaded at Palestinian Territory, occupied on December 15, 2021
www.manaraa.com

56. Walsh EJ, Miajlovic H, Gorkun OV, Foster TJ (2008) Identification of the *Staphylococcus aureus* MSCRAMM clumping factor B (ClfB) binding site in the alphaC-domain of human fibrinogen. *Microbiology* 154:550–558.
57. Nielsen HV, et al. (2012) The metal ion-dependent adhesion site motif of the *Enterococcus faecalis* EbpA pilin mediates pilus function in catheter-associated urinary tract infection. *MBio* 3:e00177-12.
58. Kato T, Kitagawa S (2006) Regulation of neutrophil functions by proinflammatory cytokines. *Int J Hematol* 84:205–209.
59. Kolaczkowska E, Kubes P (2013) Neutrophil recruitment and function in health and inflammation. *Nat Rev Immunol* 13:159–175.
60. McDonald B, Kubes P (2010) Chemokines: Sirens of neutrophil recruitment—But is it just one song? *Immunity* 33:148–149.
61. Xiang H, et al. (2012) Crystal structures reveal the multi-ligand binding mechanism of *Staphylococcus aureus* ClfB. *PLoS Pathog* 8:e1002751.
62. Nygaard TK, Pallister KB, Zurek OW, Voyich JM (2013) The impact of α-toxin on host cell plasma membrane permeability and cytokine expression during human blood infection by CA-MRSA USA300. *J Leukoc Biol* 94:971–979.
63. Watkins RL, Zurek OW, Pallister KB, Voyich JM (2013) The SaeR/S two-component system induces interferon-gamma production in neutrophils during invasive *Staphylococcus aureus* infection. *Microbes Infect* 15:749–754.
64. Rice LB (2008) Federal funding for the study of antimicrobial resistance in nosocomial pathogens: No ESKAPE. *J Infect Dis* 197:1079–1081.
65. Rosen DA, Hooton TM, Stamm WE, Humphrey PA, Hultgren SJ (2007) Detection of intracellular bacterial communities in human urinary tract infection. *PLoS Med* 4:e329.
66. Yang S, et al. (2009) Rapid identification of biothreat and other clinically relevant bacterial species by use of universal PCR coupled with high-resolution melting analysis. *J Clin Microbiol* 47:2252–2255.
67. Caporaso JG, et al. (2012) Ultra-high-throughput microbial community analysis on the Illumina HiSeq and MiSeq platforms. *ISME J* 6:1621–1624.

Downloaded at Palestinian Territory, occupied on December 15, 2021

www.manaraa.com